COMMUN. MATH. SCI.
Vol. 13, No. 5, pp. 1219–1242

MULTI-HUMP SOLITARY WAVES OF A NONLINEAR DIRAC EQUATION*

JIAN XU†, SIHONG SHAO‡, HUAZHONG TANG§, AND DONGYI WEI¶

Abstract. This paper concentrates on a (1+1)-dimensional nonlinear Dirac (NLD) equation with a general self-interaction, being a linear combination of the scalar, pseudoscalar, vector and axial vector self-interactions to the power of the integer $k+1$. The solitary wave solutions to the NLD equation are analytically derived, and the upper bounds of the hump number in the charge, energy and momentum densities for the solitary waves are proved analytically in theory. The results show that: (1) for a given integer k, the hump number in the charge density is not bigger than 4, while that in the energy density is not bigger than 3; (2) those upper bounds can only be achieved in the situation of higher nonlinearity, namely, $k\in\{5,6,7,\cdots\}$ for the charge density and $k\in\{3,5,7,\cdots\}$ for the energy density; (3) the momentum density has the same multi-hump structure as the energy density; (4) more than two humps (resp. one hump) in the charge (resp. energy) density can only happen under the linear combination of the pseudoscalar self-interaction and at least one of the scalar and vector (or axial vector) self-interactions. Our results on the multi-hump structure will be interesting in the interaction dynamics for the NLD solitary waves.

Key words. Nonlinear Dirac equation, Solitary wave, Multi-hump, Self-interaction.

AMS subject classifications. 81Q05, 37K40, 35Q51, 35L60.

1. Introduction

There is a remarkable upsurge of interest in the nonlinear Dirac (NLD) models or equations, as they emerge naturally as practical models in many physical systems, such as the extended particles in particle physics [8, 9, 13, 14], the gap solitons in nonlinear optics [3], Bose–Einstein condensates in honeycomb optical lattices [12], phenomenological models of quantum chromodynamics [7], as well as matter influencing the evolution of the universe in cosmology [26]. To make the resulting NLD model to be Lorentz invariant, the so-called self-interaction Lagrangian can be built up from the bilinear covariants which are categorised into five types: scalar, pseudoscalar, vector, axial vector and tensor. Different self-interactions give rise to different NLD models. Several interesting models have been proposed and investigated based on the scalar bilinear covariant in [10, 11, 19, 31], on the vector bilinear covariant in [33], on the axial vector bilinear covariant [18], on both scalar and pseudoscalar bilinear covariants [25], on both the scalar and vector bilinear covariants [21, 32] etc. All of these models have attracted wide interest of physicists and mathematicians, especially on looking for solitary wave solutions and investigating their physical and mathematical properties.

A key feature of the NLD equations is that it allows solitary wave solutions or particle-like solutions — the stable localized solutions with finite energy and charge [24]. That is, the particles appear as intense localized regions of fields which can be recognized as the basic ingredient in the description of extended objects in quantum field theory

*Received: November 13, 2013; accepted (in revised form): August 2, 2014. Communicated by Shi Jin.

†LMAM and School of Mathematical Sciences, Peking University, Beijing 100871, P. R. China. (xujian764@gmail.com)

‡LMAM and School of Mathematical Sciences, Peking University, Beijing 100871, P. R. China. To whom correspondence should be addressed (sihong@math.pku.edu.cn).

§HEDPS, CAPT & LMAM, School of Mathematical Sciences, Peking University, Beijing 100871, P. R. China. (hztang@math.pku.edu.cn)

¶LMAM and School of Mathematical Sciences, Peking University, Beijing 100871, P. R. China. (jnwdyi@163.com)

[34]. For the NLD equation in (1+1) dimensions (i.e. one time dimension plus one space dimension), several analytical solitary wave solutions are derived in [15] for the quadric nonlinearity, [16, 17] for fractional nonlinearity as well as [6, 32] for general nonlinearity by using explicitly the constraint resulting from the energy-momentum conservation. Most existing studies on the NLD solitary waves focus on the situation with the self-interaction Lagrangian constructed from one single bilinear covariant. For example, the Soler model [31] and the Thirring model [33] involve respectively the quadric scalar self-interaction and the quadric vector self-interaction, and further discussion about extending such two models to the situation with the integer nonlinearity is recently presented in [6, 20].

With the help of the analytical expressions of the NLD solitary wave solutions, the interaction dynamics among them can further be conveniently studied and rich nonlinear phenomena have been revealed in a series of work [1, 28, 29, 30, 35]. An important step in this direction has been made by Alvarez and Carreras [1], who simulated numerically the interaction dynamics for the (1+1)-dimensional NLD solitary waves under the quadric scalar self-interaction [2]. Shao and Tang have revisited this interaction dynamics problem [28] by employing a higher-order method. They not only reproduced the phenomena observed by Alvarez and Carreras but also observed that collapse happens in binary and ternary collisions of two-hump NLD solitary waves. Very recently, they have further investigated the interaction dynamics for the NLD solitary waves under the linear combination of scalar and vector self-interactions with the integer nonlinearity and revealed that the interaction dynamics depend on the power exponent of the self-interaction in the NLD equation. For example, collapse happens again after collision of two equal one-hump NLD solitary waves under the cubic vector self-interaction in contrast to no collapse scattering for the corresponding quadric case [35]. Their numerical results inferred that both the multi-hump (two-hump) profile and high order nonlinearity could undermine the stability during the scattering of the NLD solitary waves. Note in passing that although multi-hump solitary waves have been found for many other nonlinear models, see e.g. [22] and references therein, the detailed study of the multi-hump solitary waves of the NLD model is mostly open. Shao and Tang first pointed out the two-hump structure [28] and later work has commenced by other researchers, see e.g. [6].

In (1+1) dimensions, the pseudoscalar and tensor bilinear covariants are linearly dependent, and a direct generalization of self-interaction is linearly combining the scalar, pseudoscalar, vector and axial vector bilinear covariants with arbitrary nonlinearity, called by the linear combined self-interaction (see Equation (2.16)). A natural question is raised here: What happens for the interaction dynamics for the (1+1)-dimensional NLD solitary waves under such linear combined self-interaction? In answering the question, efficient and stable numerical methods are needed in order to solve accurately the NLD equation with the linear combined self-interaction in long time simulations. Actually, we have demonstrated that both the Runge–Kutta discontinuous Galerkin method and the exponential operator splitting method are fit for the job [29, 35]. On the other hand, more detailed information on the physical and mathematical properties of the NLD solitary waves under the linear combined self-interaction is essential to investigating the interaction dynamics. The present work will focus on studying these properties and try to answer questions such as: How to choose the coefficients of the linear combined self-interaction to make the NLD model physically significant and have solitary wave solutions? What parameters does the multi-hump structure depend on? Is the hump number related to the power exponent of the self-interaction?

The paper is organized as follows. The NLD equation with the linear combined self-interaction is introduced in Section 2 and the range of the combination coefficients is also determined there by the Hermiticity requirement of the self-interaction. In Section 3, the localized solitary wave solutions are analytically derived with the help of the conservation laws. The multi-hump structure of the charge, energy and momentum densities is analyzed in Section 4 where the upper bounds of the hump number in those densities are proved in theory. The paper is concluded in Section 5 with a few remarks.

2. Nonlinear Dirac equation

This section will introduce the (1+1)-dimensional NLD equation with the linear combined self-interaction. Throughout the paper, units in which both the speed of light and the reduced Planck constant are equal to one will be used, and the Einstein summation convection will be applied, namely, summation over repeated indices. The NLD equation has the following general covariant form

$$(\mathtt{i}\boldsymbol{\gamma}^\mu\partial_\mu - m)\boldsymbol{\Psi} + \frac{\partial L_{\mathrm{I}}}{\partial\bar{\boldsymbol{\Psi}}} = 0, \tag{2.1}$$

being the Euler–Lagrange equation $\partial_\mu\big(\partial L/\partial(\partial_\mu\bar{\boldsymbol{\Psi}})\big) - \partial L/\partial\bar{\boldsymbol{\Psi}} = 0$, where the spinor $\boldsymbol{\Psi}$ has two complex components, $\bar{\boldsymbol{\Psi}} = \boldsymbol{\Psi}^\dagger\boldsymbol{\gamma}^0$ with superscript $\dagger$ denoting the conjugate transpose, $\boldsymbol{\gamma}^\mu$ are Gamma matrices (we choose $\boldsymbol{\gamma}^0 = \sigma^z$ and $\boldsymbol{\gamma}^1 = \mathtt{i}\sigma^y$ as in [1, 28] where $\sigma^{x,y,z}$ are the standard Pauli matrices) and $\partial_\mu = \frac{\partial}{\partial x^\mu}$ for $\mu = 0$ and 1, $\mathtt{i}$ is the imaginary unit, $m \geq 0$ is the mass (the NLD model is called massive if $m > 0$ and massless if $m = 0$), and the Lagrangian L reads

$$L = L_{\mathrm{D}} + L_{\mathrm{I}}. \tag{2.2}$$

Here L_{D} denotes the Dirac Lagrangian given by

$$L_{\mathrm{D}} = \frac{\mathtt{i}}{2}\big(\bar{\boldsymbol{\Psi}}\boldsymbol{\gamma}^\mu\partial_\mu\boldsymbol{\Psi} - (\partial_\mu\bar{\boldsymbol{\Psi}})\boldsymbol{\gamma}^\mu\boldsymbol{\Psi}\big) - m\bar{\boldsymbol{\Psi}}\boldsymbol{\Psi}, \tag{2.3}$$

and the self-interaction Lagrangian L_{I} is a nonlinear functional of the spinors $\boldsymbol{\Psi}$ and $\bar{\boldsymbol{\Psi}}$, but independent of $\partial_\mu\bar{\boldsymbol{\Psi}}$, e.g. a general linear combined self-interaction in (2.16) will be considered in this work. Physically, the self-interaction Lagrangian L_{I} is not only required to be invariant under the Lorentz transformation (see Equation (4.34)), but also should be carefully chosen such that the resulting solution $\boldsymbol{\Psi}$ to the NLD Equation (2.1) satisfies the following conservation laws

$$\partial_\mu j^\mu = 0, \tag{2.4}$$

$$\partial_\mu T^{\mu\nu} = 0, \tag{2.5}$$

where the current vector j^μ and the energy-momentum tensor $T^{\mu\nu}$ are defined respectively as

$$j^\mu = \bar{\boldsymbol{\Psi}}\boldsymbol{\gamma}^\mu\boldsymbol{\Psi}, \tag{2.6}$$

$$T^{\mu\nu} = \frac{\mathtt{i}}{2}\big(\bar{\boldsymbol{\Psi}}\boldsymbol{\gamma}^\mu\partial^\nu\boldsymbol{\Psi} - (\partial^\nu\bar{\boldsymbol{\Psi}})\boldsymbol{\gamma}^\mu\boldsymbol{\Psi}\big) - \eta^{\mu\nu}L. \tag{2.7}$$

Here $\partial^\mu = \eta^{\mu\nu}\partial_\nu$ and $\eta^{\mu\nu} = \eta_{\mu\nu} = \mathrm{diag}(1,-1)$ is the Minkowski metric. Equation (2.4) corresponds to the mass conservation, while Equation (2.5) gives the energy conservation for $\nu = 0$ and the momentum conservation for $\nu = 1$. According to equations (2.4), (2.5),

(2.6) and (2.7), for the localized spinor $\mathbf{\Psi}$, integrating the zero components of the current vector j^μ and the energy-momentum tensor $T^{\mu\nu}$ yields three conserved quantities, i.e. the charge Q, the energy E, and the momentum P, as follows

$$Q=\int_{-\infty}^{+\infty} j^0 \mathrm{d}x, \tag{2.8}$$

$$E=\int_{-\infty}^{+\infty} T^{00} \mathrm{d}x, \tag{2.9}$$

$$P=\int_{-\infty}^{+\infty} T^{01} \mathrm{d}x. \tag{2.10}$$

As we have mentioned in Section 1, the self-interaction Lagrangian L_I can be built up from the bilinear covariants and several NLD models exist in the literature corresponding to different bilinear covariants. There are five types of bilinear covariants: the scalar bilinear covariant is $\bar{\mathbf{\Psi}}\mathbf{\Psi}$, the pseudoscalar bilinear covariant is $\bar{\mathbf{\Psi}}\boldsymbol{\gamma}^5\mathbf{\Psi}$, the vector bilinear covariant is $\bar{\mathbf{\Psi}}\boldsymbol{\gamma}^\mu\mathbf{\Psi}$, the axial vector bilinear covariant is $\bar{\mathbf{\Psi}}\boldsymbol{\gamma}^\mu\boldsymbol{\gamma}^5\mathbf{\Psi}$, and the tensor bilinear covariant is $\frac{\mathtt{i}}{2}\bar{\mathbf{\Psi}}(\boldsymbol{\gamma}^\mu\boldsymbol{\gamma}^\nu-\boldsymbol{\gamma}^\nu\boldsymbol{\gamma}^\mu)\mathbf{\Psi}$, where $\boldsymbol{\gamma}^5=\boldsymbol{\gamma}^0\boldsymbol{\gamma}^1$. In (1+1) dimensions, it can easily be shown that the tensor and pseudoscalar bilinear covariants are linearly dependent, e.g. $\frac{\mathtt{i}}{2}\bar{\mathbf{\Psi}}(\boldsymbol{\gamma}^1\boldsymbol{\gamma}^0-\boldsymbol{\gamma}^0\boldsymbol{\gamma}^1)\mathbf{\Psi}=-\mathtt{i}\bar{\mathbf{\Psi}}\boldsymbol{\gamma}^5\mathbf{\Psi}$, and then the remaining four bilinear covariants are used to construct the following self-interactions:

$$L_\mathrm{S}=\bar{\mathbf{\Psi}}\mathbf{\Psi}=|\Psi_1|^2-|\Psi_2|^2\in\mathbb{R}, \tag{2.11}$$

$$L_\mathrm{P}=-\mathtt{i}\bar{\mathbf{\Psi}}\boldsymbol{\gamma}^5\mathbf{\Psi}=2\mathrm{Im}(\Psi_1^*\Psi_2)\in\mathbb{R}, \tag{2.12}$$

$$L_\mathrm{V}=\bar{\mathbf{\Psi}}\boldsymbol{\gamma}^\mu\mathbf{\Psi}\bar{\mathbf{\Psi}}\boldsymbol{\gamma}_\mu\mathbf{\Psi}, \tag{2.13}$$

$$L_\mathrm{A}=\bar{\mathbf{\Psi}}\boldsymbol{\gamma}^\mu\boldsymbol{\gamma}^5\mathbf{\Psi}\bar{\mathbf{\Psi}}\boldsymbol{\gamma}_\mu\boldsymbol{\gamma}^5\mathbf{\Psi}, \tag{2.14}$$

where Ψ_1 and Ψ_2 are two components of the spinor $\mathbf{\Psi}$, the superscript $*$ denotes the complex conjugate, and $\boldsymbol{\gamma}_\mu=\eta_{\mu\nu}\boldsymbol{\gamma}^\nu$ are the covariant Gamma matrices. Further more, direct calculation shows the relation between L_V and L_A

$$L_\mathrm{V}=-L_\mathrm{A}=\left(|\Psi_1|^2+|\Psi_2|^2\right)^2-\left(2\mathrm{Re}(\Psi_1^*\Psi_2)\right)^2\geq 0. \tag{2.15}$$

Thus the general linear combined self-interaction can be formally written as

$$L_\mathrm{I}=s(L_\mathrm{S})^{k+1}+p(L_\mathrm{P})^{k+1}+v(L_\mathrm{V})^{\frac{1}{2}(k+1)}, \tag{2.16}$$

where the exponent power $k+1$ is an integer, and the linear combination coefficients s,p,v should be carefully chosen such that the resulting NLD models are physically meaningful. For some special choice of the parameters k,s,p,v, Equation (2.16) will reduce to the often-cited NLD models in literature such as the Thirring model [5, 33] and the Soler or Gross-Neveu model [10, 31]. If the spinor $\mathbf{\Psi}$ is scaled by a constant factor as $\widetilde{\mathbf{\Psi}}=\sqrt{\alpha}\mathbf{\Psi}$ with $\alpha\in\mathbb{C}$, then the scaled self-interaction Lagrangian will be $\alpha^{k+1}L_\mathrm{I}[\mathbf{\Psi}]$ which shows that the power exponent to α is $k+1$. In this sense, we say that the self-interaction Lagrangian L_I has the power exponent $k+1$, for example, the quadric and cubic self-interaction are referred to the case $k=1$ and the case $k=2$, respectively. The linear combination of the quadric scalar and quadric pseudoscalar self-interactions has been studied in [15, 25], while the linear combination of the scalar and vector self-interactions with a general power exponent has been considered in [32, 35]. The linear combined self-interaction (2.16) with $k=1$ has also been mentioned in [23].

Obviously, the linear combined self-interaction L_{I} in (2.16) is Lorentz invariant because each of $L_{\mathrm{S}}, L_{\mathrm{P}}, L_{\mathrm{V}}$ is invariant under the Lorentz transformation. Accordingly, the only remaining physical requirement is to choose the linear combination coefficients in (2.16) such that the resulting NLD spnior $\boldsymbol{\Psi}$ satisfies the conservation laws (2.4) and (2.5). It can readily be shown that the linear combined self-interaction (2.16) satisfies the so-called homogeneity relation [17, 32]

$$\bar{\boldsymbol{\Psi}}\frac{\partial L_{\mathrm{I}}}{\partial \bar{\boldsymbol{\Psi}}} = (k+1)L_{\mathrm{I}}, \quad \left(\frac{\partial L_{\mathrm{I}}}{\partial \bar{\boldsymbol{\Psi}}}\right)^{\dagger}\boldsymbol{\gamma}^0\boldsymbol{\Psi} = (k+1)L_{\mathrm{I}}^*. \tag{2.17}$$

Combining equations (2.1), (2.6) and (2.17) gives that the conservation law (2.4) is equivalent to the Hermiticity of the linear combined self-interaction (2.16), i.e.

$$L_{\mathrm{I}} = L_{\mathrm{I}}^*, \tag{2.18}$$

which poses a requirement the self-interaction (2.16) must satisfy. Multiplying Equation (2.1) from the left with $\bar{\boldsymbol{\Psi}}$ plus the conjugate transpose of Equation (2.1) multiplied with $\boldsymbol{\gamma}^0\boldsymbol{\Psi}$ from the right yields

$$2L_{\mathrm{D}} + \bar{\boldsymbol{\Psi}}\frac{\partial L_{\mathrm{I}}}{\partial \bar{\boldsymbol{\Psi}}} + \left(\frac{\partial L_{\mathrm{I}}}{\partial \bar{\boldsymbol{\Psi}}}\right)^{\dagger}\boldsymbol{\gamma}^0\boldsymbol{\Psi} = 0,$$

for Equation (2.3), and then we have the useful relation

$$L = -kL_{\mathrm{I}}, \tag{2.19}$$

for equations (2.2), (2.17) and (2.18). In consequence, combining the homogeneity relation (2.17), the relation (2.19) between L and L_{I} as well as the Hermiticity requirement (2.18), and direct algebraic calculation leads to the conservation law (2.5). That is, the spinor $\boldsymbol{\Psi}$ of the NLD Equation (2.1) with the linear combined self-interaction (2.16) follows the conservation laws (2.4) and (2.5) if and only if the Hermiticity requirement (2.18) is satisfied. Below we will use the Hermiticity requirement (2.18) to choose the linear combination coefficients in (2.16). Before that, we would like to make a remark that the cases of $k=-1$ and $k=0$ will not be considered in the following because the NLD Equation (2.1) degenerates to the linear Dirac equation when $k=-1$ according to Equation (2.17), and the Lagrangian L vanishes (i.e. $L\equiv 0$) when $k=0$ for the relation (2.19).

The Hermiticity condition (2.18) implies

$$(s-s^*)(L_{\mathrm{S}})^{k+1} + (p-p^*)(L_{\mathrm{P}})^{k+1} + (v-v^*)(L_{\mathrm{V}})^{\frac{1}{2}(k+1)} = 0, \tag{2.20}$$

for $k\in\mathbb{Z}\setminus\{-1,0\}$ and $L_{\mathrm{S}}, L_{\mathrm{P}}, L_{\mathrm{V}}$ are all real as shown in equations (2.11), (2.12) and (2.15). In particular, for the quadric case (i.e. $k=1$), Equation (2.20) further reduces to

$$(s-p-s^*+p^*)(L_{\mathrm{S}})^2 + (v+p-v^*-p^*)L_{\mathrm{V}} = 0, \tag{2.21}$$

on account of $(L_{\mathrm{P}})^2 = L_{\mathrm{V}} - (L_{\mathrm{S}})^2$ [23]. Because of the arbitrariness of the NLD spinor $\boldsymbol{\Psi}$, Equation (2.21) implies that both $s-p$ and $v+p$ must be real when $k=1$, otherwise s, p, v must all be real for $k\in\mathbb{Z}\setminus\{0,\pm 1\}$. The range of the parameters $\{s,p,v\}$ in the

linear combined self-interaction (2.16) with a given integer power exponent $k+1$ reads as follows

$$\mathcal{E}_k := \begin{cases} \{(s,p,v)|s-p\in\mathbb{R}, v+p\in\mathbb{R}, |s-p|+|v+p|\neq 0\} & \text{for} \quad k=1, \\ \{(s,p,v)|s\in\mathbb{R}, p\in\mathbb{R}, v\in\mathbb{R}, |s|+|p|+|v|\neq 0\} & \text{for} \quad k\in\mathbb{Z}\setminus\{0,\pm 1\}, \end{cases} \tag{2.22}$$

where the coefficients with which $L_{\mathrm{I}}\equiv 0$ holds have been excluded.

In the next section, for $k\in\mathbb{Z}\setminus\{-1,0\}$, we are going to look for the localized solitary wave solutions for the NLD Equation (2.1) with the linear combined self-interaction (2.16) of a given integer power exponent $k+1$ under the condition that the linear combination coefficients in Equation (2.16) belong to $\mathcal{E}_k$ in Equation (2.22).

3. Solitary wave solutions

This section will focus on seeking the localized solutions of the following form for the (1+1)-dimensional NLD Equation (2.1) with (2.16) in the spirit of the methods used in [4, 15, 17, 32]. The solution with the form

$$\boldsymbol{\Psi}(x,t)=\mathrm{e}^{-\mathtt{i}\omega t}\boldsymbol{\psi}(x), \quad \boldsymbol{\psi}(x)=\begin{pmatrix}\varphi(x)\\ \chi(x)\end{pmatrix} \tag{3.1}$$

is wanted, where $\omega\geq 0$ is the frequency, and both $|\varphi(x)|$ and $|\chi(x)|$ are required to decay very fast to zero as $|x|\to+\infty$. Such solutions are said to be localized in $\mathbb{R}$ as mentioned before. Substituting the *ansatz* (3.1) into the Lagrangian (2.2) and the energy-momentum tensor (2.7) gives respectively

$$L=\omega\bar{\boldsymbol{\psi}}\boldsymbol{\gamma}^0\boldsymbol{\psi}+\frac{\mathtt{i}}{2}(\bar{\boldsymbol{\psi}}\boldsymbol{\gamma}^1\partial_x\boldsymbol{\psi}-(\partial_x\bar{\boldsymbol{\psi}})\boldsymbol{\gamma}^1\boldsymbol{\psi})-m\bar{\boldsymbol{\psi}}\boldsymbol{\psi}+L_{\mathrm{I}}, \tag{3.2}$$

$$T^{00}=-\frac{\mathtt{i}}{2}(\bar{\boldsymbol{\psi}}\boldsymbol{\gamma}^1\partial_x\boldsymbol{\psi}-(\partial_x\bar{\boldsymbol{\psi}})\boldsymbol{\gamma}^1\boldsymbol{\psi})+m\bar{\boldsymbol{\psi}}\boldsymbol{\psi}-L_{\mathrm{I}}, \tag{3.3}$$

$$T^{01}=-\frac{\mathtt{i}}{2}(\bar{\boldsymbol{\psi}}\boldsymbol{\gamma}^0\partial_x\boldsymbol{\psi}-(\partial_x\bar{\boldsymbol{\psi}})\boldsymbol{\gamma}^0\boldsymbol{\psi}), \tag{3.4}$$

$$T^{10}=\omega\bar{\boldsymbol{\psi}}\boldsymbol{\gamma}^1\boldsymbol{\psi}, \tag{3.5}$$

$$T^{11}=\omega\bar{\boldsymbol{\psi}}\boldsymbol{\gamma}^0\boldsymbol{\psi}-m\bar{\boldsymbol{\psi}}\boldsymbol{\psi}+L_{\mathrm{I}}, \tag{3.6}$$

all of which are independent of the time t in this moment, and thus the conservation law (2.5) becomes

$$\frac{\mathrm{d}T^{10}}{\mathrm{d}x}=\frac{\mathrm{d}T^{11}}{\mathrm{d}x}=0,$$

which implies that

$$T^{10}=T^{11}=0 \tag{3.7}$$

for the localized solutions (3.1), i.e.

$$\omega\bar{\boldsymbol{\psi}}\boldsymbol{\gamma}^1\boldsymbol{\psi}=0, \tag{3.8}$$

$$\omega\boldsymbol{\psi}^\dagger\boldsymbol{\psi}-m\bar{\boldsymbol{\psi}}\boldsymbol{\psi}+L_{\mathrm{I}}=0. \tag{3.9}$$

To ensure Equation (3.8), we require

$$\bar{\boldsymbol{\psi}}\boldsymbol{\gamma}^1\boldsymbol{\psi}=\varphi^*\chi+\varphi\chi^*=0. \tag{3.10}$$

That is, $\varphi^*\chi$ is imaginary. To this end, we assume that φ is real and χ is imaginary as follows

$$\begin{pmatrix}\varphi(x)\\ \chi(x)\end{pmatrix}=R(x)\begin{pmatrix}\cos(\theta(x))\\ \mathtt{i}\sin(\theta(x))\end{pmatrix}, \tag{3.11}$$

where both $R(x)$ and $\theta(x)$ are under-determined real functions. Only the classical solutions are considered below and both $R(x)$ and $\theta(x)$ at least belong to $C^1(\mathbb{R})$ which consists of all differentiable functions in $\mathbb{R}$ whose derivative is continuous. Meanwhile, we assume that for any $x\in\mathbb{R}$, the charge density $j_0(x)$ does not vanish, that means, the particle described by the NLD spinor $\mathbf{\Psi}$ in Equation (3.1) has a positive probability to go anywhere in $\mathbb{R}$. Under such assumption, according to Equation (2.6), for any $x\in\mathbb{R}$, we have $R(x)\neq 0$ for

$$\rho_Q(x):=j^0[\mathbf{\Psi}](x,t)=\boldsymbol{\psi}^\dagger(x)\boldsymbol{\psi}(x)=(R(x))^2>0, \tag{3.12}$$

where the spinor $\mathbf{\Psi}$ is given in Equation (3.1) and the notation $\rho_Q(x)$ denoting the charge density has been introduced for convenience. Moreover, physically, the charge Q defined in Equation (2.8) is required to be finite, i.e. $Q=\int_{-\infty}^{+\infty}\rho_Q(x)\mathrm{d}x<+\infty$. Note in passing that substituting Equation (3.11) into Equation (3.4) directly leads to

$$T^{01}=0 \tag{3.13}$$

which means the momentum density vanishes for all $x\in\mathbb{R}$. Further substituting equations (3.1) and (3.11) into equations (2.11), (2.12) and (2.13) leads to, respectively,

$$L_{\mathrm{S}}=\bar{\boldsymbol{\psi}}(x)\boldsymbol{\psi}(x)=(R(x))^2\cos(2\theta(x)), \tag{3.14}$$

$$L_{\mathrm{P}}=(R(x))^2\sin(2\theta(x)), \tag{3.15}$$

$$L_{\mathrm{V}}=(R(x))^4, \tag{3.16}$$

and then the linear combined self-interaction (2.16) becomes

$$L_{\mathrm{I}}=(R(x))^{2(k+1)}G(x), \tag{3.17}$$

where

$$G(x):=s(\cos(2\theta(x)))^{k+1}+p(\sin(2\theta(x)))^{k+1}+v, \tag{3.18}$$

is introduced for convenience.

Combining equations (2.19), (3.2) and (3.9) yields

$$k\omega\boldsymbol{\psi}^\dagger\boldsymbol{\psi}-km\bar{\boldsymbol{\psi}}\boldsymbol{\psi}-\frac{\mathtt{i}}{2}(\bar{\boldsymbol{\psi}}\boldsymbol{\gamma}^1\boldsymbol{\psi}_x-\bar{\boldsymbol{\psi}}_x\boldsymbol{\gamma}^1\boldsymbol{\psi})=0, \tag{3.19}$$

which does not depend on the particular type of the self-interaction involved and could be solved analytically. Substituting the *ansatz* (3.11) into (3.19) gives rise to the ordinary differential equation

$$\frac{\mathrm{d}\theta(x)}{m\cos(2\theta(x))-\omega}=k\mathrm{d}x, \tag{3.20}$$

under the condition of $m\cos(2\theta(x))-\omega\neq 0$, otherwise $\theta(x)=\frac{1}{2}\cos^{-1}\frac{\omega}{m}$. According to the integral formula

$$\int_{u_0}^{u}\frac{\mathrm{d}\theta}{a+b\cos(c\theta)}\quad(c\neq 0)=\begin{cases}\frac{2}{c\sqrt{b^2-a^2}}\tanh^{-1}\left(\frac{(b-a)}{\sqrt{b^2-a^2}}\tan\left(\frac{cu}{2}\right)\right), & |b|>|a|,\\ -\frac{1}{ac}\cot\left(\frac{cu}{2}\right), & b=-a\neq 0,\\ \frac{2}{c\sqrt{a^2-b^2}}\tan^{-1}\left(\frac{(a-b)}{\sqrt{a^2-b^2}}\tan\left(\frac{cu}{2}\right)\right), & |b|<|a|,\\ \frac{1}{ac}\tan\left(\frac{cu}{2}\right), & b=a\neq 0,\end{cases} \tag{3.21}$$

where the value of u_0 is taken to be π/c for the second case and to be zero for the remaining three cases, the solution of (3.20) can be obtained as follows:

- When $m>\omega\geq 0$, the solution of (3.20) with $\theta(0)=0$ is

$$\theta(x)=\tan^{-1}(\alpha\tanh(k\beta x))\in\left(-\tan^{-1}(\alpha),\tan^{-1}(\alpha)\right)\subseteq\left(-\frac{\pi}{4},\frac{\pi}{4}\right), \tag{3.22}$$

  where

$$\alpha=\sqrt{\frac{m-\omega}{m+\omega}},\quad \beta=\sqrt{m^2-\omega^2}. \tag{3.23}$$

- When $\omega=m>0$, the solution of (3.20) with $\theta(0)=\frac{\pi}{2}$ is

$$\theta(x)=\cot^{-1}(2mkx)\in(0,\pi). \tag{3.24}$$

- When $\omega>m\geq 0$, the solution of (3.20) with $\theta(0)=0$ is

$$\theta(x)=\tan^{-1}\left(\sqrt{\frac{\omega-m}{\omega+m}}\tan\left(-k\sqrt{\omega^2-m^2}x\right)\right)\in\left(-\frac{\pi}{2},\frac{\pi}{2}\right). \tag{3.25}$$

Note in passing that the solution (3.25) can also be reformulated into the solution (3.22) using the properties: $\tanh(\mathtt{i}x)=\mathtt{i}\tan(x)$ and $\tan(-x)=-\tan(x)$, and the last case of the integral formula (3.21) cannot happen in Equation (3.20) since both m and ω are nonnegative. The remaining task is to solve $R(x)$.

Further combining equations (3.9), (3.12), (3.14) and (3.17) yields

$$(R(x))^{2k}G(x)=m\cos(2\theta(x))-\omega, \tag{3.26}$$

from which we can conclude that either $G(x)\equiv 0$ in $\mathbb{R}$ (i.e. $L_I\equiv 0$ for Equation (3.17) and will not be considered) or $G(x)\neq 0$ for all $x\in\mathbb{R}$ holds, namely, either Ω_0 or Ω_1 equals to $\mathbb{R}$ after denoting $\Omega_0:=\{x|G(x)=0\}$ and $\Omega_1:=\{x|G(x)\neq 0\}$, and the demonstration is as follows. For $m\geq 0$ and $\omega\geq 0$, there are only four cases to investigate: $m=\omega=0$, $\omega>m\geq 0$, $m>\omega\geq 0$ and $m=\omega>0$. For all $x\in\mathbb{R}$, we have $R(x)\neq 0$, and $m\cos(2\theta(x))-\omega=0$ for $m=\omega=0$ or $m\cos(2\theta(x))-\omega<0$ for $\omega>m\geq 0$, thus $G(x)=0$ holds in the case of $m=\omega=0$, while $G(x)\neq 0$ is true for the case of $\omega>m\geq 0$. When $m>\omega\geq 0$, if there exists $x_0<x_1\in\mathbb{R}$ such that $x_0\in\Omega_0$ and $x_1\in\Omega_1$, then we have: on the one hand, from Equation (3.26), $\cos(2\theta(x))=\frac{\omega}{m}$ holds for all $x\in[x_0,x_1]\cap\Omega_0$; on the other hand, from Equation (3.22), there exits $M>0$ and $\delta=\frac{1-(\alpha\tanh(k\beta M))^2}{1+(\alpha\tanh(k\beta M))^2}>\frac{1-\alpha^2}{1+\alpha^2}=\frac{\omega}{m}$ such that $\cos(2\theta(x))\geq\delta$ holds for all $x\in[x_0,x_1]\cap\Omega_1$. This contradicts the assumption that $\theta(x)$ as well as $\cos(2\theta(x))$ are continuous in $[x_0,x_1]$. The discussion of the remaining case of $m=\omega>0$ is similar to that of the case of $m>\omega\geq 0$. Below we will concentrate on the situation of $G(x)\neq 0$ as well as $m\cos(2\theta(x))-\omega\neq 0$ for all $x\in\mathbb{R}$. From Equation (3.26), $R(x)$ is solved in $\mathbb{R}$ as follows

$$R(x)=\pm\left(\frac{m\cos(2\theta(x))-\omega}{G(x)}\right)^{\frac{1}{2k}}, \tag{3.27}$$

which expresses $R(x)$ in terms of $\theta(x)$ for Equation (3.18), while $\theta(x)$ has been solved in equations (3.22), (3.24) and (3.25). Consequently, according to Equation (3.12), the charge density becomes

$$\rho_Q(x)=\left(\frac{m\cos(2\theta(x))-\omega}{G(x)}\right)^{\frac{1}{k}}. \tag{3.28}$$

It is worth noting that the derivation of the above solution $\mathbf{\Psi}(x,t)$ given in Equation (3.1) with equations (3.11), (3.22), (3.24), (3.25) and (3.27) is referred to as sufficient and logically complete, that is to say, the above function $\mathbf{\Psi}(x,t)$ satisfies the (1+1)-dimensional NLD Equation (2.1) with the self-interaction (2.16). Its demonstration is easy through directly substituting $\mathbf{\Psi}(x,t)$ into (2.1) with (2.16) and some algebraic manipulations.

The physical solutions with which the charge Q is finite (i.e. $Q<+\infty$ implying $\lim_{x\to\infty}\rho_Q(x)=0$ must be true) will be selected from equations (3.22), (3.24), (3.25) and (3.27). On the one hand, we discard the case of $k\in\{-2,-3,-4,\cdots\}$ in which the limit of $\rho_Q(x)$ cannot be zero as $x\to\infty$ and the reason is as follows. For example, when $m>\omega\geq 0$ and $k<-1$, the parameter p must be zero (otherwise $G(0)$ will be infinity and then $\rho_Q(x)$ will be discontinuous at $x=0$ according to Equation (3.28)), and from Equation (3.18) we have $G(x)=s(\cos(2\theta(x)))^{k+1}+v$, thus $\lim_{x\to+\infty}(m\cos(2\theta(x))-\omega)=0$ for Equation (3.22) and $\lim_{x\to+\infty}G(x)=s(\frac{\omega}{m})^{k+1}+v$. In consequence, from Equation (3.28), it is evident that $\rho_Q(x)$ will diverge as $x\to\infty$ if $s(\frac{\omega}{m})^{k+1}+v\neq 0$. In the case of $s(\frac{\omega}{m})^{k+1}+v=0$ which implies that s cannot be zero, directly using L'Hospital's rule gives $\lim_{x\to+\infty}\rho_Q(x)=\left(\frac{m}{s(k+1)}\right)^{\frac{1}{k}}\frac{m}{\omega}\neq 0$. On the other hand, the case of $k\in\mathbb{Z}^+$ and $\omega>m\geq 0$ is also discarded and the reason is, in such case, we have both $m\cos(2\theta(x))-\omega\leq m-\omega<0$ and $|G(x)|\leq|s|+|p|+|v|$ hold for all $x\in\mathbb{R}$, thus there exists $\delta=\left(\frac{\omega-m}{|s|+|p|+|v|}\right)^{\frac{1}{k}}>0$ such that $\rho_Q(x)>\delta$ holds for all $x\in\mathbb{R}$. Therefore, the physical solutions may exist only in the situation of $k\in\mathbb{Z}^+$ and $m\geq\omega\geq 0$ and will be searched in the following.

3.1. $k\in\mathbb{Z}^+$ **and** $m>\omega\geq 0$**.** This subsection focuses on the situation with $k\in\mathbb{Z}^+$ and $m>\omega\geq 0$, in which $\theta(x)$ is given in Equation (3.22) and monotonously increases from $-\tan^{-1}(\alpha)$ to $\tan^{-1}(\alpha)$ as x goes from $-\infty$ to $+\infty$. Then we have

$$m\cos 2\theta-\omega=\frac{\alpha\beta\,\mathrm{sech}^2(k\beta x)}{1+(\alpha\tanh(k\beta x))^2}\in(0,m-\omega], \tag{3.29}$$

and thus $1\geq\cos 2\theta>\frac{\omega}{m}\geq 0$. In order to facilitate the subsequent discussion, we introduce an intermediate function $y(x)=\tanh(k\beta x)$ which increases monotonously from -1 to 1 when x goes from $-\infty$ to $+\infty$ and thus $\lim_{x\to\pm\infty}y(x)=\pm 1$. The dependence of $y(x)$ and $\theta(x)$ on x is implicitly implied hereafter. From Equation (3.22), we have the relation

$$y=\frac{1}{\alpha}\tan(\theta),\quad \cos(2\theta)=\frac{1-\alpha^2y^2}{1+\alpha^2y^2},\quad \sin(2\theta)=\frac{2\alpha y}{1+\alpha^2y^2}, \tag{3.30}$$

and then rewrite $G(x)$ given in Equation (3.18) and $\rho_Q(x)$ given in Equation (3.28) in terms of y into $\tilde{G}(y)$ and $\tilde{\rho}_Q(y)$, respectively, as follows

$$\tilde{G}(y)=s\left(\frac{1-\alpha^2y^2}{1+\alpha^2y^2}\right)^{k+1}+p\left(\frac{2\alpha y}{1+\alpha^2y^2}\right)^{k+1}+v, \tag{3.31}$$

$$\tilde{\rho}_Q(y)=(\alpha\beta)^{\frac{1}{k}}\left(\frac{1-y^2}{1+\alpha^2y^2}\right)^{\frac{1}{k}}\left(\frac{1}{\tilde{G}(y)}\right)^{\frac{1}{k}}, \tag{3.32}$$

and $\rho_Q(x)>0$ shown in Equation (3.28) gives

$$\forall y\in(-1,1),\quad \tilde{G}(y)>0. \tag{3.33}$$

Then the charge Q becomes

$$Q=\frac{(\alpha\beta)^{\frac{1}{k}}}{k\beta}I(\alpha,k), \tag{3.34}$$

where

$$I(\alpha,k):=\int_{-1}^{1}\frac{(1-y^2)^{\frac{1}{k}-1}}{\left((1+\alpha^2y^2)\tilde{G}(y)\right)^{\frac{1}{k}}}\mathrm{d}y. \tag{3.35}$$

Because $\alpha,\beta\in(0,+\infty)$ and $k\in\mathbb{Z}^+$, the finite charge condition is equivalent to

$$I(\alpha,k)<\infty, \tag{3.36}$$

and the necessary condition $\lim\limits_{x\to\infty}\rho_Q(x)=0$ implies

$$\lim_{y\to\pm1}\tilde{\rho}_Q(y)=0. \tag{3.37}$$

In short, we should seek the solution in the situation with $k\in\mathbb{Z}^+$ and $m>\omega\geq0$ satisfying the restrictions (3.33) and (3.36). Given $(s,p,v)\in\mathcal{E}_k$, the foregoing restrictions are used to determine the feasible set for ω, and the discussion is split into two cases: one is for $k=1$, the other is for $k\in\{2,3,4,\cdots\}$.

• When $k=1$, the inequality (3.33) becomes:

$$\tilde{G}(y)=(s-p)\left(\frac{1-\alpha^2y^2}{1+\alpha^2y^2}\right)^2+v+p>0$$

holds for any $y\in(-1,1)$. It is equivalent to both $\tilde{G}(0)>0$ and $\tilde{G}(1)\geq0$ since $\tilde{G}(y)$ is even with respect to $y\in(-1,1)$ and increases monotonously when $s-p\leq0$ and decreases monotonously when $s-p>0$ as y increases in $[0,1)$. If $\tilde{G}(1)=0$, then

$$\lim_{y\to\pm1}\tilde{\rho}_Q(y)=\frac{\beta(1+\alpha^2)}{2\alpha\left((s-p)(1-\alpha^2)-(v+p)(1+\alpha^2)\right)}\neq0,$$

which violates the necessary condition (3.37), and thus we require $\tilde{G}(1)>0$. Therefore, for a given $\omega\in\mathcal{F}_1$, there exists $\epsilon=\min\{\tilde{G}(0),\tilde{G}(1)\}>0$ such that

$$I(\alpha,1)\leq\frac{1}{\epsilon}\int_{-1}^{1}\frac{1}{1+\alpha^2y^2}\mathrm{d}y\leq\frac{2}{\epsilon}<\infty,$$

where the set $\mathcal{F}_1$ is define by

$$\mathcal{F}_1:=\{\omega|\omega\in[0,m),\tilde{G}(0)>0,\tilde{G}(1)>0\}. \tag{3.38}$$

That is, the feasible set of ω for the case of $k=1$ is $\mathcal{F}_1$.

• When $k\in\{2,3,4,\cdots\}$, if $\tilde{G}(1)=0$, then

$$\lim_{y\to1}\tilde{\rho}_Q(y)=\left(\frac{\beta(1+\alpha^2)^k}{(k+1)(s\alpha(1-\alpha^2)^k-p(2\alpha)^k-v\alpha(1+\alpha^2)^k)}\right)^{\frac{1}{k}}\neq0,$$

and if $\tilde{G}(-1)=0$, then

$$\lim_{y\to -1}\tilde{\rho}_Q(y)=\left(\frac{\beta(1+\alpha^2)^k}{(k+1)(s\alpha(1-\alpha^2)^k+p(-2\alpha)^k-v\alpha(1+\alpha^2)^k)}\right)^{\frac{1}{k}}\neq 0,$$

both of which violate the necessary condition (3.37). Thus, the feasible set for ω in the case of $k\in\{2,3,4,\cdots\}$ should be a subset of the following set

$$\mathcal{F}_k:=\{\omega|\omega\in[0,m),\forall y\in[-1,1],\tilde{G}(y)>0\},\text{ for } k\in\{2,3,4,\cdots\}.$$

Since $\tilde{G}(y)$ has at most three extreme points at $0,\pm\frac{1}{\alpha}\tan\left(\frac{1}{2}\tan^{-1}\left|\frac{s}{p}\right|^{\frac{1}{k-1}}\right)$ for $y\in(-1,1)$, the minimum of $\tilde{G}(y)$ must locate among these three extreme points and the two endpoints. In consequence, we have equivalently

$$\mathcal{F}_k=\{\omega|\omega\in[0,m),\forall y\in\mathcal{P},\tilde{G}(y)>0\},\text{ for } k\in\{2,3,4,\cdots\},\tag{3.39}$$

where

$$\mathcal{P}:=\left\{0,\pm1,\pm\frac{1}{\alpha}\tan\left(\frac{1}{2}\tan^{-1}\left|\frac{s}{p}\right|^{\frac{1}{k-1}}\right)\right\}\cap[-1,1]$$

is a finite set of no more than five elements. It can be readily verified that, for a given $\omega\in\mathcal{F}_k$ with $k\in\{2,3,4,\cdots\}$, there exists $\epsilon=\min_{y\in[-1,1]}\{\tilde{G}(y)\}>0$ such that

$$I(\alpha,k)\leq\frac{1}{\epsilon^{\frac{1}{k}}}\int_{-1}^{1}(1-y^2)^{\frac{1}{k}-1}\mathrm{d}y=\frac{\sqrt{\pi}\Gamma\left(\frac{1}{k}\right)}{\epsilon^{\frac{1}{k}}\Gamma\left(\frac{1}{2}+\frac{1}{k}\right)}<\infty,$$

where $\Gamma(x)$ is the gamma function. That is, the feasible set of ω for the case of $k\in\{2,3,4,\cdots\}$ is indeed $\mathcal{F}_k$ given in Equation (3.39).

REMARK 3.1. Generally, $\mathcal{F}_k\subsetneqq[0,m)$ holds for most cases of $(s,p,v)\in\mathcal{E}_k$ with $k\in\mathbb{Z}^+$. For the NLD solitary waves with the scalar and vector self-interaction and $s>0$, $-s<v\leq 0$, $p=0$, the feasible set becomes $\mathcal{F}_k=\left(\left(\frac{-v}{s}\right)^{\frac{1}{k+1}}m,m\right)$ for any $k\in\mathbb{Z}^+$, while for those with only the pseudoscalar self-interaction (i.e. $s=0$, $p\neq 0$, $v=0$), the feasible set becomes $\mathcal{F}_k=\varnothing$ for all $k\in\mathbb{Z}^+$.

3.2. $k\in\mathbb{Z}^+$ and $\omega=m>0$. This subsection concerns the situation with $k\in\mathbb{Z}^+$ and $\omega=m>0$ in which $\theta(x)$ is given in Equation (3.24). Consequently, we have

$$\cos 2\theta=\frac{(2kmx)^2-1}{(2kmx)^2+1}\in[-1,1),\tag{3.40}$$

$$\sin 2\theta=\frac{4kmx}{(2kmx)^2+1}\in[-1,1],$$

$$G(x)=s\left(\frac{(2kmx)^2-1}{(2kmx)^2+1}\right)^{k+1}+p\left(\frac{4kmx}{(2kmx)^2+1}\right)^{k+1}+v,$$

$$m\cos 2\theta-\omega=-\frac{2m}{(2kmx)^2+1}\in[-2m,0),\tag{3.41}$$

and the charge density becomes

$$j_0(x)=\left(-\frac{2m}{(1+(2kmx)^2)G(x)}\right)^{\frac{1}{k}},\tag{3.42}$$

with $|G(x)|<|s|+|p|+|v|$. Since $j_0(x)>0$ as shown in Equation (3.12), we obtain

$$G(x)<0, \quad \forall x\in(-\infty,+\infty). \tag{3.43}$$

Since $j_0(x)\propto\frac{1}{x^{2/k}}(x\to\infty)$, the finite charge condition requires $0<k<2$. It is worth noting that $j_0(x)$ decays polynomially to zero as $x\to\infty$, which is completely different from the exponential decay described in Section 3.1. Therefore, we only need to consider the case of $k=1$ in which the restriction (3.43) becomes:

$$\forall x\in(-\infty,\infty),\ G(x)=(s-p)\left(\frac{(2mx)^2-1}{(2mx)^2+1}\right)^2+v+p<0,$$

that is equivalent to requiring $G(0)=s+v<0$ as well as $G\left(\frac{1}{2m}\right)=v+p<0$ since $G(x)$ is even and has three local extreme points $x=0,\pm\frac{1}{2m}$, and $\lim\limits_{x\to\infty}G(x)=s+v=G(0)$. Accordingly, we have

$$Q=\frac{\pi}{\sqrt{(s+v)(v+p)}}, \tag{3.44}$$

i.e. the charge is finite. Hence for $\omega=m>0$ and $k=1$, we have that the NLD solitary waves displayed in equations (3.1) and (3.11) satisfy the finite charge condition if the linear combination coefficients (s,p,v) belong to

$$\mathcal{E}_1^-:=\{(s,p,v)|s+v<0,v+p<0\}\subset\mathcal{E}_1,$$

otherwise, the charge corresponding to the NLD spinor given in equations (3.1) and (3.11) cannot be finite or Equation (3.12) cannot hold for all $x\in\mathbb{R}$.

Remark 3.2. It was pointed out that the profile of the charge density $\rho_Q(x)$ given in Equation (3.28) is either one-hump or two-hump under only the quadric scalar self-interaction (i.e. $k=1$, $v=p=0$) [28], which is still true for the scalar self-interaction with more general integer exponent power (i.e. $k>1$, $v=p=0$) [6]. The role such multi-hump structures play in the interaction dynamics for the NLD solitary waves attracts a lot of attention. Numerical results have shown that the two-hump NLD solitary waves may collapse (i.e. they after collision stop being solitary waves) during the scattering, whereas the collapse phenomena cannot be generally observed in collisions of the one-hump NLD solitary waves [28, 30]. Since the collision can be regarded as a solution of the time-dependent equation with the initial condition formed by two or more solitary waves separated from each other by large distances, so as to be independent, we conjecture, the "instability" is related to such collapses. More efforts are still needed in exploring the physical mechanism of the collapse, such as when and why the NLD solitary waves may collapse during their interaction dynamics. A more direct question is naturally raised: Is there a connection between the instability (i.e. collapse) and the multi-hump structure? Very recently, the stability was studied in [27] by numerical simulations using the fourth-order operator splitting integration method [35]. It was observed there that all stable NLD solitary waves have a one-hump profile, but not all one-hump waves are stable, while all waves with two humps are unstable. We have further shown that collapse happens after binary collision of one-hump NLD solitary waves under the cubic self-interaction in contrast to no collapse scattering for the corresponding quadric case [35].

In summary, both the multi-hump (two-hump) structure and high order nonlinearity could undermine the stability during the scattering of the NLD solitary waves. In the next section, we will show that the multi-hump structure depends on the linear combination coefficients $(s,p,v)\in\mathcal{E}_k$ and the integer power exponent $k+1$.

4. Multi-hump structure

This section will focus on investigating the multi-hump structure of the NLD solitary wave (3.1) with the linear combined self-interaction (2.16) for $(s,p,v)\in\mathcal{E}_k$ and $\omega\in\mathcal{F}_k$ when $k\in\mathbb{Z}^+$ and $m>\omega\geq 0$ as well as for $(s,p,v)\in\mathcal{E}_1^-$ when $k=1$ and $m=\omega>0$. More specifically, we will answer: Can the charge density $\rho_Q(x)$ have more humps than two under the linear combined self-interaction (2.16)? At most how many humps can the charge density $\rho_Q(x)$ afford? Can we have similar results for the energy density or the momentum density?

4.1. $k\in\mathbb{Z}^+$ **and** $m>\omega\geq 0$**.** The number of humps in the charge density $\rho_Q(x)$ is equal to the number of its local maximum and can be determined by the number of zeros of $\frac{\mathrm{d}\rho_Q(x)}{\mathrm{d}x}$, and the zeros of $\frac{\mathrm{d}\rho_Q(x)}{\mathrm{d}x}$ are the same as those of $\frac{\mathrm{d}\rho_Q^k(x)}{\mathrm{d}x}$ for $\rho_Q(x)>0$ and $k\in\mathbb{Z}^+$. When $m>\omega\geq 0$, for convenience, we introduce an intermediate variable $\xi=2\theta$ and rewrite $\rho_Q(x)$ in terms of ξ into

$$\hat{\rho}_Q(\xi)=m^{\frac{1}{k}}\left(\frac{\cos\xi-a}{\hat{G}(\xi)}\right)^{\frac{1}{k}}>0,\quad \forall\xi\in I, \tag{4.1}$$

where

$$\begin{aligned} a&:=\frac{\omega}{m}\in[0,1),\\ \hat{G}(\xi)&:=s\cos^{k+1}\xi+p\sin^{k+1}\xi+v,\\ I&:=(-\cos^{-1}(a),\cos^{-1}(a))\subset\left(-\frac{\pi}{2},\frac{\pi}{2}\right). \end{aligned}$$

Combining equations (3.20), (3.29) and (3.30) gives that $\frac{\mathrm{d}\xi}{\mathrm{d}x}>0$ holds for all $x\in\mathbb{R}$, and then the chain rule

$$\frac{\mathrm{d}\rho_Q^k(x)}{\mathrm{d}x}=\frac{\mathrm{d}\hat{\rho}_Q^k(\xi)}{\mathrm{d}\xi}\frac{\mathrm{d}\xi}{\mathrm{d}x}=-\hat{\rho}_Q^{2k}(\xi)\frac{\mathrm{d}\hat{\rho}_Q^{-k}(\xi)}{\mathrm{d}\xi}\frac{\mathrm{d}\xi}{\mathrm{d}x} \tag{4.2}$$

further implies that $\frac{\mathrm{d}\rho_Q^k(x)}{\mathrm{d}x}$ has the same zeros as $\frac{\mathrm{d}\hat{\rho}_Q^{-k}(\xi)}{\mathrm{d}\xi}$. That is, the remaining task is to determine or estimate the number of zeros of $\frac{\mathrm{d}\hat{\rho}_Q^{-k}(\xi)}{\mathrm{d}\xi}$. To this end, technically, we need the following two lemmas in which $\#_\Omega^z[f]$ (resp. $\#_\Omega^e[f]$) represents the number of zeros (resp. extreme points at which the derivatives of $f(\xi)$ are zero) of the function $f(\xi)\in C^1(\Omega)$ in an open interval Ω.

LEMMA 4.1. Given $f(\xi)\in C^1(\Omega)$, we have

(i) $\#_\Omega^z[f]\leq\#_\Omega^e[f]+1$;

(ii) $\#_\Omega^z[\alpha f]=\#_\Omega^z[f]$ and $\#_\Omega^e[\alpha f]=\#_\Omega^e[f]$ hold for any $\alpha\neq 0$.

LEMMA 4.2. Suppose $f(\xi),g(\xi),\frac{g'(\xi)}{f'(\xi)}\in C^1(\Omega)$, and $f(\xi)\neq 0$ holds for all $\xi\in\Omega$. Then

$$\#_\Omega^e\left[\frac{g}{f}\right]\leq\#_\Omega^e\left[\frac{g'}{f'}\right]+\#_\Omega^z[f']+1.$$

Proof. The identity $\left(\frac{g'}{f'}f-g\right)'=\left(\frac{g'}{f'}\right)'f$ implies

$$\#_\Omega^e\left[\frac{g'}{f'}f-g\right]=\#_\Omega^e\left[\frac{g'}{f'}\right], \tag{4.3}$$

since $f(\xi)\neq 0$ holds for all $\xi\in\Omega$. Similarly, since $\left(\frac{g}{f}\right)' = \frac{f'}{f^2}\left(\frac{g'}{f'}f-g\right)$, then

$$\begin{aligned}\#^e_\Omega\left[\frac{g}{f}\right] &\leq \#^z_\Omega\left[\frac{g'}{f'}f-g\right]+\#^z_\Omega[f'] \\ &\leq \#^e_\Omega\left[\frac{g'}{f'}f-g\right]+1+\#^z_\Omega[f'] \\ &\leq \#^e_\Omega\left[\frac{g'}{f'}\right]+\#^z_\Omega[f']+1,\end{aligned}$$

where we have used Lemma 4.1(i) in the second line and Equation (4.3) in the last line. □

We are now in position to determine $\#^e_I\left[\hat{\rho}_Q^{-k}\right]$, i.e. the number of extreme points of $\hat{\rho}_Q^{-k}(\xi)$ in the interval I. Because

$$\hat{\rho}_Q^{-k}(\xi) = \frac{1}{m}\frac{\hat{G}(\xi)}{\cos\xi - a} =: \frac{1}{m}\frac{g_1(\xi)}{f_1(\xi)}, \tag{4.4}$$

for Equation (4.1), using Lemma 4.1(ii) and Lemma 4.2 directly gives

$$\#^e_I\left[\hat{\rho}_Q^{-k}\right] = \#^e_I\left[\frac{1}{m}\frac{g_1}{f_1}\right] = \#^e_I\left[\frac{g_1}{f_1}\right] \leq \#^e_I\left[\frac{g_1'}{f_1'}\right]+\#^z_I[f_1']+1. \tag{4.5}$$

A direct calculation shows

$$\begin{aligned}g_1'(\xi) &= (k+1)(-s\cos^k\xi\sin\xi + p\sin^k\xi\cos\xi), \\ f_1'(\xi) &= -\sin\xi,\end{aligned} \tag{4.6}$$

thus

$$\#^z_I[f_1'] = 1, \tag{4.7}$$

and

$$\frac{g_1'(\xi)}{f_1'(\xi)} = \frac{(k+1)(s-p\tan^{k-1}\xi)}{\cos^{-k}\xi} =: (k+1)\frac{g_2(\xi)}{f_2(\xi)} \tag{4.8}$$

which implies by Lemma 4.1(ii) and Lemma 4.2 that

$$\#^e_I\left[\frac{g_1'}{f_1'}\right] = \#^e_I\left[(k+1)\frac{g_2}{f_2}\right] = \#^e_I\left[\frac{g_2}{f_2}\right] \leq \#^e_I\left[\frac{g_2'}{f_2'}\right]+\#^z_I[f_2']+1, \tag{4.9}$$

for $k\in\mathbb{Z}^+$. It can easily be shown that

$$\begin{aligned}g_2'(\xi) &= -p(k-1)\tan^{k-2}\xi\cos^{-2}\xi, \\ f_2'(\xi) &= k\cos^{-k-1}\xi\sin\xi,\end{aligned} \tag{4.10}$$

and then

$$\#^z_I[f_2'] = 1, \tag{4.11}$$

$$\frac{g_2'(\xi)}{f_2'(\xi)} = -\frac{p(k-1)}{k}\sin^{k-3}\xi\cos\xi, \tag{4.12}$$

$$\left(\frac{g_2'(\xi)}{f_2'(\xi)}\right)' = -\frac{p(k-1)}{k}\sin^{k-4}\xi\left((k-3)\cos^2\xi-\sin^2\xi\right). \tag{4.13}$$

Based on the foregoing derivation, we can rigorously determine the number of humps of the charge density $\rho_Q(x)$ and the results are summarized as follows.

• **Case Q1**: When $k\in\mathbb{Z}^+$ and $s=p=0$, we have $v\neq 0$ for $(s,p,v)\in\mathcal{E}_k$ and Equation (4.4) becomes

$$\hat{\rho}_Q^{-k}(\xi) = \frac{v}{m}\frac{1}{\cos\xi-a},$$

from which it can readily be seen that the charge density has only one hump.

• **Case Q2**: When $k\in\mathbb{Z}^+$, $p=0$ and $s\neq 0$, Equation (4.8) becomes

$$\frac{g_1'(\xi)}{f_1'(\xi)} = (k+1)s\cos^k\xi,$$

then we have $\#_I^e\left[\frac{g_1'}{f_1'}\right]=1$, thus $\#_I^e\left[\hat{\rho}_Q^{-k}\right]\leq 3$ for Equation (4.5), i.e. the charge density has at most two humps.

• **Case Q3**: When $k=1$ and $s=p\neq 0$, Equation (4.4) becomes

$$\hat{\rho}_Q^{-1}(\xi) = \frac{s+v}{m}\frac{1}{\cos\xi-a},$$

from which it can readily be seen that the charge density has only one hump.

• **Case Q4**: When $k=1$, $p\neq 0$ and $s\neq p$, Equation (4.8) becomes

$$\frac{g_1'(\xi)}{f_1'(\xi)} = 2(s-p)\cos\xi,$$

and we have $\#_I^e\left[\frac{g_1'}{f_1'}\right]=1$, thus $\#_I^e\left[\hat{\rho}_Q^{-1}\right]\leq 3$ for Equation (4.5), i.e. the charge density $\rho_Q(x)$ has at most two humps.

• **Case Q5**: When $k=2$ and $p\neq 0$, Equation (4.8) becomes

$$\frac{g_1'(\xi)}{f_1'(\xi)} = 3(s\cos^2\xi-p\sin\xi\cos\xi),$$

then we have

$$\left(\frac{g_1'(\xi)}{f_1'(\xi)}\right)' = -3(s\sin(2\xi)+p\cos(2\xi)),$$

and $\#_I^e\left[\frac{g_1'}{f_1'}\right]\leq 2$, thus $\#_I^e\left[\hat{\rho}_Q^{-2}\right]\leq 4$ for Equation (4.5), i.e. the charge density $\rho_Q(x)$ has at most two humps.

• **Case Q6**: When $k=3$ and $p\neq 0$, Equation (4.12) becomes

$$\frac{g_2'(\xi)}{f_2'(\xi)} = -\frac{2p}{3}\cos\xi,$$

then we have $\#_I^e\left[\frac{g_2'}{f_2'}\right]=1$, thus $\#_I^e\left[\hat{\rho}_Q^{-3}\right]\leq 5$ for equations (4.5), (4.7), (4.9) and (4.11), i.e. the charge density has at most three humps.

• **Case Q7**: When $k=4$ and $p\neq 0$, Equation (4.13) becomes

$$\left(\frac{g_2'(\xi)}{f_2'(\xi)}\right)'=-\frac{3p}{4}\cos(2\xi),$$

which implies that $\frac{g_2'(\xi)}{f_2'(\xi)}$ has at most two extreme points, then we have $\#_I^e\left[\frac{g_2'}{f_2'}\right]\leq 2$, thus $\#_I^e\left[\hat{\rho}_Q^{-4}\right]\leq 6$, for equations (4.5), (4.7), (4.9) and (4.11), which means that the charge density has at most three humps.

• **Case Q8**: When $k\in\{5,6,7,\cdots\}$ and $p\neq 0$, Equation (4.13) implies that the extreme points of $\frac{g_2'(\xi)}{f_2'(\xi)}$ possibly locate at $\xi=0$ and $\xi=\pm\tan^{-1}(\sqrt{k-3})$ and thus

$$\#_I^e\left[\frac{g_2'}{f_2'}\right]\leq 3. \tag{4.14}$$

Combining equations (4.5), (4.7), (4.9), (4.11) and (4.14) leads to

$$\#_I^e\left[\hat{\rho}_Q^{-k}\right]\leq 7, \tag{4.15}$$

which means that the charge density has at most four humps.

Remark 4.3. Our analysis has shown that: (i) the charge density has only one hump under the pure vector self-interaction [6] and has either one hump or two humps under the linear combination of the scalar and vector self-interactions [35]; (ii) The charge density has at most four humps for $(s,p,v)\in\mathcal{E}_k$ and $\omega\in\mathcal{F}_k$ when $k\in\mathbb{Z}^+$ and $m>\omega\geq 0$; (iii) The NLD solitary wave with the four-hump charge density can only appear in the situation of higher nonlinearity, i.e. $k\in\{5,6,7,\cdots\}$, while for the case of $k\in\{1,2\}$ (resp. $k\in\{3,4\}$), the charge density has at most two (resp. three) humps; (iv) under the linear combination of the vector and pseudoscalar self-interactions (i.e. $v\neq 0,p\neq 0,s=0$) with $k\in\{3,4,5\cdots\}$ the charge density also has at most three humps because setting $s=0$ in Equation (4.8) leads to

$$\left(\frac{g_1'(\xi)}{f_1'(\xi)}\right)'=((k-1)\cot^2\xi-1)\sin^k\xi,$$

which has at most three zeros, i.e. $\#_I^e\left[\frac{g_1'}{f_1'}\right]\leq 3$, then $\#_I^e\left[\hat{\rho}_Q^{-k}\right]\leq 5$ for equations (4.5) and (4.7); (v) The charge density can indeed have three humps or four humps as shown in figures 4.1 and 4.2, while the two-hump charge density was first pointed out in [28].

Apart from the charge Q in (2.8), there are another two important conservative quantities: the energy E in (2.9) and the momentum P in (2.10). For the solitary wave solutions with the form in equations (3.1) and (3.11), from Equation (3.13), the momentum density $\rho_P(x):=T^{01}[\mathbf{\Psi}](x,t)$ in Equation (3.4) vanishes for all $x\in\mathbb{R}$, which reflects that the NLD solitary waves are at rest (i.e. the standing waves), while the energy density $\rho_E(x):=T^{00}[\mathbf{\Psi}](x,t)$ in (3.3) becomes

$$\rho_E(x)=\rho_Q(x)(mk\cos(2\theta(x))-(k-1)\omega)>0,\quad \forall x\in\mathbb{R}, \tag{4.16}$$

for equations (3.9), (3.19), (3.1) and (3.11). Next, we are going to investigate the multi-hump structure of the energy density $\rho_E(x)$ and the method is similar to that used in discussing the multi-hump structure of the charge density $\rho_Q(x)$.

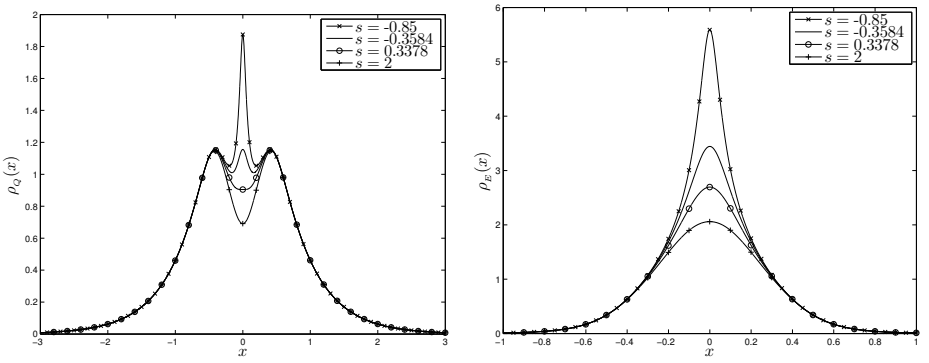

(a) The charge density $\rho_Q(x)$. (b) The energy density $\rho_E(x)$.

Fig. 4.1: *The two-hump and three-hump charge densities are plotted in (a) with respect to s with other parameters being* $m=1,k=3,\omega=0.01,v=1,p=-0.95$. *The critical value for the two-hump charge densities transiting to the three-hump ones is* $s=\frac{25}{74}\simeq 0.3378$. *When* $s\simeq -0.3584$, *the three peaks have the same height* 1.156 *and locate at* $x=0$ *and* $x\simeq\pm 0.4110$. *It is noted that the energy densities with the same parameters have just one hump, see (b).*

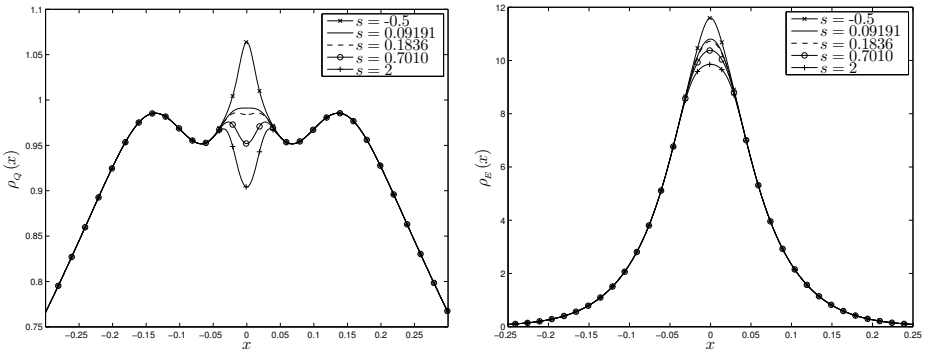

(a) The charge density $\rho_Q(x)$. (b) The energy density $\rho_E(x)$.

Fig. 4.2: *The three-hump and four-hump charge densities are plotted in (a) with respect to s with other parameters being* $m=1,k=11,\omega=0.01,v=1,p=-0.95$. *The critical value for the three-hump charge densities transiting to the four-hump ones is* $s=\frac{25}{272}\simeq 0.09191$. *The four peaks have the same height for* $s\simeq 0.1836$ *and so do the three valleys for* $s\simeq 0.7010$. *It is noted that the energy densities with the same parameters have only one hump, see (b).*

Rewrite $\rho_E(x)$ in terms of the intermediate variable ξ into

$$\hat{\rho}_E(\xi)=mk\hat{\rho}_Q(\xi)(\cos\xi-b)>0,\quad \forall\xi\in I, \tag{4.17}$$

where $b=\frac{k-1}{k}a\le a$ and Equation (4.1) is applied, and the number of extreme points of $\hat{\rho}_E^{-k}(\xi)$ in the interval I, i.e. $\#_I^e\left[\hat{\rho}_E^{-k}\right]$, is to be estimated. Because

$$\hat{\rho}_E^{-k}(\xi)=\frac{1}{m^{k+1}k^k}\frac{\hat{G}(\xi)}{(\cos\xi-a)(\cos\xi-b)^k}=\frac{1}{m^{k+1}k^k}\frac{g_1(\xi)}{h_1(\xi)}, \tag{4.18}$$

for equations (4.4) and (4.17), where $h_1(\xi):=(\cos\xi-a)(\cos\xi-b)^k$, using Lemma 4.1(ii)

and Lemma 4.2 gives

$$\#_I^e\left[\hat{\rho}_E^{-k}\right]=\#_I^e\left[\frac{1}{m^{k+1}k^k}\frac{g_1}{h_1}\right]=\#_I^e\left[\frac{g_1}{h_1}\right]\le\#_I^e\left[\frac{g_1'}{h_1'}\right]+\#_I^z[h_1']+1. \tag{4.19}$$

A direct calculation shows

$$h_1'(\xi)=-\sin\xi(\cos\xi-b)^{k-1}(k+1)(\cos\xi-c), \tag{4.20}$$

where $c=\frac{ka+b}{k+1}=\frac{k(k+1)-1}{k(k+1)}a$ and $\cos\xi-b\ge\cos\xi-c\ge\cos\xi-a>0$ holds for all $\xi\in I$, thus

$$\#_I^z[h_1']=1. \tag{4.21}$$

Combining equations (4.6), (4.8) and (4.20) leads to

$$\frac{g_1'(\xi)}{h_1'(\xi)}=\frac{s-p\tan^{k-1}\xi}{(1-\frac{b}{\cos\xi})^{k-1}(1-\frac{c}{\cos\xi})}=\frac{g_2(\xi)}{h_2(\xi)}, \tag{4.22}$$

where $h_2(\xi):=(1-\frac{b}{\cos\xi})^{k-1}(1-\frac{c}{\cos\xi})$. By Lemma 4.2, Equation (4.22) implies that

$$\#_I^e\left[\frac{g_1'}{h_1'}\right]=\#_I^e\left[\frac{g_2}{h_2}\right]\le\#_I^e\left[\frac{g_2'}{h_2'}\right]+\#_I^z[h_2']+1. \tag{4.23}$$

It can easily be shown that

$$h_2'(\xi)=-(1-\tfrac{b}{\cos\xi})^{k-2}\tfrac{\sin\xi}{\cos^2\xi}\left(b(k-1)(1-\tfrac{c}{\cos\xi})+c(1-\tfrac{b}{\cos\xi})\right), \tag{4.24}$$

thus we have

$$\#_I^z[h_2']=1,\quad \text{if } b\ne0, \tag{4.25}$$

and

$$\frac{g_2'(\xi)}{h_2'(\xi)}=p\frac{(k-1)\sin^{k-3}\xi}{(\cos\xi-b)^{k-2}\left(b(k-1)(1-\frac{c}{\cos\xi})+c(1-\frac{b}{\cos\xi})\right)}, \tag{4.26}$$

for Equation (4.10). Hence we are able to determine the number of humps of the energy density $\rho_E(x)$ and the results are shown below.

• **Case E1**: When $k\in\mathbb{Z}^+$ and $p=\omega=0$, Equation (4.18) becomes

$$\hat{\rho}_E^{-k}(\xi)=\frac{1}{m^{k+1}k^k}\left(s+\frac{v}{\cos^{k+1}\xi}\right),$$

from which it can readily be seen that the energy density has only one hump.

• **Case E2**: When $k\in\mathbb{Z}^+$, $p=0$ and $\omega\ne0$, we have $0<\omega<m$, $a>0$, $b>0$, and Equation (4.18) becomes

$$\hat{\rho}_E^{-k}(\xi)=\frac{1}{m^{k+1}k^k}\frac{q_1(\xi)}{q_2(\xi)}, \tag{4.27}$$

where

$$q_1(\xi):=s+\tfrac{v}{\cos^{k+1}\xi},\quad\text{and}\quad q_2(\xi):=(1-\tfrac{a}{\cos\xi})(1-\frac{b}{\cos\xi})^k.$$

It is easy to show that both $q_1(\xi)$ and $q_2(\xi)$ are even and positive in the domain I. In fact, we can further show that $\frac{q_1(\xi)}{q_2(\xi)}$ increases monotonously as ξ goes from 0 to $\cos^{-1}a$ which implies that the energy density has only one hump in this situation. The reason is given in the following. The case of $v\geq 0$ is trivial. If $v<0$, then we have $s>0$ for $\hat{G}(0)=s+v>0$ because $\omega\in\mathcal{F}_k$, and using the formula for difference of powers leads to

$$q_1(\xi)=\left(\rho-\frac{\eta}{\cos\xi}\right)\sum_{j=0}^{k}\rho^j\left(\frac{\eta}{\cos\xi}\right)^{k-j}, \tag{4.28}$$

where $\rho:=s^{\frac{1}{k+1}}>0$ and $\eta:=(-v)^{\frac{1}{k+1}}>0$. It is simple to see that $\rho-\frac{\eta}{\cos\xi}>0$ holds for all $x\in[0,\cos^{-1}a)$ and the limit gives $a\rho-\eta\geq 0$ when $\xi\to\cos^{-1}a$. Combining equations (4.27) and (4.28) yields

$$\frac{q_1(\xi)}{q_2(\xi)}=\left(\frac{a\rho-\eta}{a(1-\frac{a}{\cos\xi})(1-\frac{b}{\cos\xi})^k}+\frac{\eta}{a(1-\frac{b}{\cos\xi})^k}\right)\sum_{j=0}^{k}\rho^j\left(\frac{\eta}{\cos\xi}\right)^{k-j}, \tag{4.29}$$

where the identity $\rho-\frac{\eta}{\cos\xi}=\rho-\frac{\eta}{a}+\frac{\eta}{a}\left(1-\frac{a}{\cos\xi}\right)$ is applied. From Equation (4.29), it is trivial to see that $\frac{q_1(\xi)}{q_2(\xi)}$ increases monotonously in the domain $[0,\cos^{-1}a)$.

• **Case E3**: When $k=1$ and $p\neq 0$, we have

$$\hat{\rho}_E^{-1}=\frac{1}{m^2}\frac{(s-p)+\frac{v+p}{\cos^2\xi}}{(1-\frac{a}{\cos\xi})(1-\frac{b}{\cos\xi})}$$

and thus the energy density also has only one hump by utilizing an argument similar to that used in the situation of $k\in\mathbb{Z}^+$ and $p\neq 0$ (see above **Case E1** and **Case E2**).

• **Case E4**: When $k\in\{2,3,4,\cdots\}$, $p\neq 0$ and $\omega=0$, we have $a=b=0$, and Equation (4.22) becomes

$$\frac{g_1'(\xi)}{h_1'(\xi)}=s-p\tan^{k-1}\xi,$$

which implies that $\#_I^e\left[\frac{g_1'}{h_1'}\right]\leq 1$ and thus $\#_I^e\left[\hat{\rho}_E^{-k}\right]\leq 3$ for equations (4.19) and (4.21). That is, the energy density has at most two humps.

• **Case E5**: When $k=2$, $p\neq 0$ and $\omega\neq 0$, Equation (4.22) becomes

$$\frac{1}{p}\frac{g_2(\xi)}{h_2(\xi)}=\frac{\frac{s}{p}-\tan\xi}{(1-\frac{b}{\cos\xi})(1-\frac{c}{\cos\xi})}, \tag{4.30}$$

from which it is easy to see that $\frac{1}{p}\frac{g_2(\xi)}{h_2(\xi)}$ decreases monotonously as ξ goes from $-\cos^{-1}a$ to $\cos^{-1}a$ when $s=0$ or as ξ goes from $-\cos^{-1}a$ to 0 when $\frac{s}{p}>0$, and $\xi=0$ is not the extreme point of $\frac{1}{p}\frac{g_2(\xi)}{h_2(\xi)}$ for

$$\left(\frac{1}{p}\frac{g_2(\xi)}{h_2(\xi)}\right)'_{\xi=0}=-\frac{1}{(1-b)(1-c)}<0.$$

That is, $\#_I^e\left[\frac{g_2}{h_2}\right]=0$ holds for $s=0$ and $\#_I^e\left[\frac{g_2}{h_2}\right]=\#_{I_1}^e\left[\frac{g_2}{h_2}\right]$ is true for $\frac{s}{p}>0$ where $I_1=(0,\cos^{-1}a)$. When $\frac{s}{p}>0$, using Lemma 4.2 further gives

$$\#_I^e\left[\frac{g_2}{h_2}\right]=\#_{I_1}^e\left[\frac{g_2}{h_2}\right]\leq\#_{I_1}^e\left[\frac{g_2'}{h_2'}\right]+\#_{I_1}^z[h_2']+1\leq 2, \tag{4.31}$$

where in the last inequality we have used $\#_{I_1}^z[h_2']=0$ for Equation (4.24) as well as $\#_{I_1}^e\left[\frac{g_2'}{h_2'}\right]\leq 1$ for

$$\left(\frac{g_2'(\xi)}{h_2'(\xi)}\right)'=\frac{p(2bc-(b+c)\cos^3\xi)}{(h_2'(\xi)\cos^3\xi)^2}.$$

By a similar argument, we can easily show that $\#_I^e\left[\frac{g_2}{h_2}\right]\leq 2$ also holds for $\frac{s}{p}<0$. Therefore, $\#_I^e\left[\frac{g_2}{h_2}\right]\leq 2$ is always true and thus we have $\#_I^e\left[\hat{\rho}_E^{-k}\right]\leq 4$ for equations (4.19), (4.21) and (4.22), which means that the energy density has at most two humps.

• **Case E6**: When $k\in\{3,5,7,\cdots\}$, $p\neq 0$ and $\omega\neq 0$, from Equation (4.26), we find that $\frac{1}{p}\frac{g_2'(\xi)}{h_2'(\xi)}$ is even and increases monotonously as ξ goes from 0 to $\cos^{-1}a$, then $\#_I^e\left[\frac{g_2'}{h_2'}\right]=1$ and $\#_I^e\left[\hat{\rho}_E^{-k}\right]\leq 5$ for equations (4.19), (4.21), (4.23) and (4.25), which means that the energy density has at most three humps.

• **Case E7**: When $k\in\{4,6,8,\cdots\}$, $p\neq 0$ and $\omega\neq 0$, from Equation (4.26), we find that $\frac{1}{p}\frac{g_2'(\xi)}{h_2'(\xi)}$ is odd and increases monotonously as ξ goes from 0 to $\cos^{-1}a$, then $\#_I^e\left[\frac{g_2'}{h_2'}\right]=0$ and $\#_I^e\left[\hat{\rho}_E^{-k}\right]\leq 4$ for equations (4.19), (4.21), (4.23) and (4.25), which means that the energy density has at most two humps.

REMARK 4.4. Our analysis has shown that: (i) the energy density has only one hump under the linear combination of the scalar and vector self-interactions; (ii) The energy density has at most three humps for $(s,p,v)\in\mathcal{E}_k$ and $\omega\in\mathcal{F}_k$ when $k\in\mathbb{Z}^+$ and $m>\omega\geq 0$; (iii) The NLD solitary wave with the three-hump energy density can only appear in the situation of higher nonlinearity of even power, i.e. $k\in\{3,5,7,\cdots\}$, while for the case of $k\in\{2,4,6,\cdots\}$, the energy density has at most two humps; (iv) under the linear combination of the vector and pseudoscalar self-interactions (i.e. $v\neq 0,p\neq 0,s=0$) with $k\in\{3,5,7\cdots\}$, the energy density also has at most two humps because setting $s=0$ in Equation (4.22) leads to

$$-\frac{1}{p}\frac{g_1'(\xi)}{h_1'(\xi)}=\frac{\tan^{k-1}\xi}{(1-\frac{b}{\cos\xi})^{k-1}(1-\frac{c}{\cos\xi})},$$

which is even and increases monotonously as ξ goes from 0 to $\cos^{-1}a$, then $\#_I^e\left[\frac{g_1'}{h_1'}\right]=1$ and $\#_I^e\left[\hat{\rho}_E^{-k}\right]\leq 3$ for equations (4.19) and (4.21); (v) The energy density can indeed have two humps or three humps as shown in Figure 4.3.

Everything we have discussed above is about the standing wave (i.e. the velocity $V=0$) from which we can obtain the moving wave (i.e. $0<V<1$) by the Lorentz boost (see equations (4.33) and (4.34)) in terms of variable of ϕ as follows

$$\tanh\phi=V,\ \cosh\phi=\gamma,\ \sinh\phi=\gamma V,\ \cosh\frac{\phi}{2}=\sqrt{\frac{\gamma+1}{2}},\ \sinh\frac{\phi}{2}=\sqrt{\frac{\gamma-1}{2}},\tag{4.32}$$

where $\gamma:=\frac{1}{\sqrt{1-V^2}}$ is the Lorentz factor. The resulting relation between the right moving wave denoted by $\mathbf{\Psi}^{\rm mw}$ and the standing wave denoted by $\mathbf{\Psi}^{\rm sw}$ in equations (3.1) and (3.11) reads

$$\mathbf{\Psi}^{\rm mw}(x,t)=\boldsymbol{S}\mathbf{\Psi}^{\rm sw}(\tilde{x},\tilde{t}),\quad \boldsymbol{S}:=\begin{pmatrix}\cosh\frac{\phi}{2} & \sinh\frac{\phi}{2}\\ \sinh\frac{\phi}{2} & \cosh\frac{\phi}{2}\end{pmatrix},\tag{4.33}$$

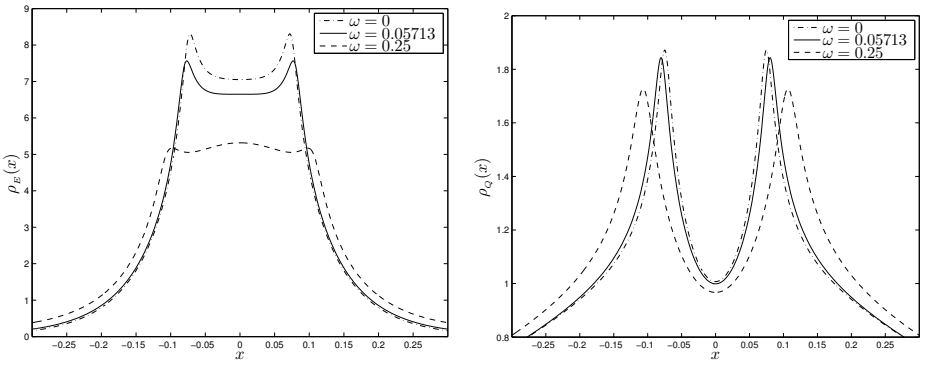

(a) The energy density $\rho_E(x)$. (b) The charge density $\rho_Q(x)$.

Fig. 4.3: *The two-hump and three-hump energy densities are plotted in (a) with respect to ω with other parameters being $m=1$, $s=1$, $p=0.25$, $v=-0.05$, $k=7$. The critical value for the two-hump energy densities transiting to the three-hump ones is $\omega=\frac{1035-\sqrt{856185}}{1920}\simeq 0.05713$. It is noted that the charge densities with the same parameters have only two humps, see (b).*

where

$$\begin{pmatrix} t \\ x \end{pmatrix} = \mathbf{\Lambda} \begin{pmatrix} \tilde{t} \\ \tilde{x} \end{pmatrix}, \quad \mathbf{\Lambda} := \begin{pmatrix} \cosh\phi & \sinh\phi \\ \sinh\phi & \cosh\phi \end{pmatrix}, \tag{4.34}$$

is the so-called Lorentz transformation between the moving frame (x,t) and the rest frame $(\tilde{x},\tilde{t})$ [28, 35]. Combining equations (2.6), (3.1), (3.10) and (4.33) yields

$$j^0[\mathbf{\Psi}^{\rm mw}](x,t) = \gamma j^0[\mathbf{\Psi}^{\rm sw}](\tilde{x},\tilde{t}). \tag{4.35}$$

Moreover, it is straightforward to show that

$$\partial^\mu = \Lambda^\mu_{\tilde{\mu}}\partial^{\tilde{\mu}},\ \boldsymbol{S}^\dagger\boldsymbol{\gamma}^0 = \boldsymbol{\gamma}^0\boldsymbol{S}^{-1},\ \boldsymbol{S}^{-1}\boldsymbol{\gamma}^\mu\boldsymbol{S} = \Lambda^\mu_{\tilde{\mu}}\boldsymbol{\gamma}^{\tilde{\mu}},\ \eta^{\mu\nu} = \Lambda^\mu_{\tilde{\mu}}\Lambda^\nu_{\tilde{\nu}}\eta^{\tilde{\mu}\tilde{\nu}},$$

where $\Lambda^\mu_{\tilde{\mu}}$ is the $(\mu,\tilde{\mu})$ entry of $\mathbf{\Lambda}$ in Equation (4.34), and then

$$T^{\mu\nu}[\mathbf{\Psi}^{\rm mw}](x,t) = \Lambda^\mu_{\tilde{\mu}}\Lambda^\nu_{\tilde{\nu}}T^{\tilde{\mu}\tilde{\nu}}[\mathbf{\Psi}^{\rm sw}](\tilde{x},\tilde{t}), \tag{4.36}$$

from which we can readily verify

$$T^{00}[\mathbf{\Psi}^{\rm mw}](x,t) = \gamma^2 T^{00}[\mathbf{\Psi}^{\rm sw}](\tilde{x},\tilde{t}), \tag{4.37}$$

$$T^{01}[\mathbf{\Psi}^{\rm mw}](x,t) = V\gamma^2 T^{00}[\mathbf{\Psi}^{\rm sw}](\tilde{x},\tilde{t}), \tag{4.38}$$

for equations (3.7), (3.13) and (4.32). It is easy to see that, Equation (4.35) (resp. (4.37)) implies the charge (resp. energy) density for $\mathbf{\Psi}^{\rm mw}$ has the same multi-hump structure as that for $\mathbf{\Psi}^{\rm sw}$, while the momentum density for $\mathbf{\Psi}^{\rm mw}$ has the same multi-hump structure as the energy density for Equation (4.38).

4.2. $k=1$ **and** $\omega=m>0$**.** When $k=1$, $\omega=m>0$ and $(s,p,v)\in\mathcal{E}_1^-$, the profile of the charge density $\rho_Q(x)$ has either one hump or two humps. The reason is shown as follows. Recall from the discussion in Section 4.1 that the number of humps in the

charge density $\rho_Q(x)$ can be determined by the number of zeros of $\frac{\mathrm{d}\rho_Q(x)}{\mathrm{d}x}$ which has the form

$$\frac{\mathrm{d}\rho_Q(x)}{\mathrm{d}x}=\frac{16m^3x}{(G(x))^2}\left(s+v-\frac{4(s-p)}{(4m^2x^2+1)^2}\right), \tag{4.39}$$

for Equation (3.42). From Equation (4.39), it is easy to see that the charge density has three extreme points at $x=0, x=\pm\frac{\sqrt{\sqrt{\frac{4(s-p)}{s+v}}-1}}{2m}$ (i.e. two humps) if $3s-4p-v<0$, otherwise has only one hump at $x=0$. As for the energy density, combining equations (3.40) (3.42) and (4.16) leads to

$$\rho_E(x)=\frac{2m^2(1-(2mx)^2)}{(s-p)((2mx)^2-1)^2+(v+p)((2mx)^2+1)^2},$$

then

$$\frac{\mathrm{d}\rho_E(x)}{\mathrm{d}x}=\frac{16m^4x\left((s+v)(4m^2x^2-1)^2-4(v+p)\right)}{\left((s-p)((2mx)^2-1)^2+(v+p)((2mx)^2+1)^2\right)^2},$$

from which we have that the energy density $\rho_E(x)$ has two humps at $x=\pm\frac{\sqrt{1-2\sqrt{\frac{v+p}{s+v}}}}{2m}$ if $3v+4p-s>0$, otherwise has only one hump at $x=0$. From equations (4.35) and (4.37), we have that the charge or energy density for the moving wave has the same multi-hump structure as that for the standing wave as shown above. According to Equation (4.38), the momentum density for the moving wave also has the same multi-hump structure as the energy density.

5. Conclusion

In this study, the NLD solitary waves under the linear combined self-interaction to the power of the integer $k+1$ have been analytically derived and the multi-hump structure in the charge, energy and momentum densities has been rigorously analyzed. We have proved that for a given integer k, the number of solitary humps for the charge density is bounded above by 4, while that for the energy density is bounded above by 3. Besides the two-hump structure first reported in [28], the three-hump and four-hump charge densities have been observed. We have also proved that the four-hump charge density can only exist in the situation of higher nonlinearity, i.e. $k\in\{5,6,7,\cdots\}$, while the three-hump one can appear in the situation of $k\in\{3,4,5,\cdots\}$. The three-hump energy density which can only occur in the situation of $k\in\{3,5,7,\cdots\}$ has also been pointed out. It has been shown that the momentum density has the same multi-hump structure as the energy density. Our analysis has further revealed that, the linear combined self-interaction in which $p\neq0$ as well as at least one of s,v is not zero is crucial for generating more than two humps (resp. one hump) in the charge (resp. energy) density. Actually, under the pure scalar self-interaction (i.e. $s\neq0,\ p=v=0$), the charge density can be either one-hump or two-hump while the energy density can only be one-hump; under the pure vector self-interaction (i.e. $v\neq0,\ s=p=0$), both the charge density and the energy density have only one hump; under the linear combination of the scalar and vector self-interactions (i.e. $s\neq0, v\neq0,\ p=0$), the charge density can be either one-hump or two-hump while the energy density can only be one-hump; no physical solutions exist under the pure pseudoscalar self-interaction (i.e. $p\neq0,\ s=v=0$). In addition, when $k=1$ and $\omega=m>0$, the NLD solitary wave with polynomial decay exists and to our knowledge, it has not been reported before this work.

Acknowledgement. The research of this work was partly supported by grants from the National Natural Science Foundation of China (Project Nos. 10925101, 11101011, 11421101, 11471025 and 91330110) and the Specialized Research Fund for the Doctoral Program of Higher Education (Project No. 20110001120112).

REFERENCES

[1] A. Alvarez and B. Carreras, *Interaction dynamics for the solitary waves of a nonlinear Dirac model*, Phys. Lett. A, 86, 327–332, 1981.
[2] A. Alvarez, P.Y. Kuo, and L. Vázquez, *The numerical study of a nonlinear one-dimensional Dirac equation*, Appl. Math. Comput., 13, 1–15, 1983.
[3] I.V. Barashenkov, D.E. Pelinovsky, and E.V. Zemlyanaya, *Vibrations and oscillatory instabilities of gap solitons*, Phys. Rev. Lett., 80, 5117–5120, 1998.
[4] S.J. Chang, S.D. Ellis, and B.W. Lee, *Chiral confinement: An exact solution of the massive Thirring model*, Phys. Rev. D, 11, 3572–3582, 1975.
[5] S. Coleman, *Quantum sine-Gordon equation as the massive Thirring model*, Phys. Rev. D, 11, 2088–2097, 1975.
[6] F. Cooper, A. Khare, B. Mihaila, and A. Saxena, *Solitary waves in the nonlinear Dirac equation with arbitrary nonlinearity*, Phys. Rev. E, 82, 036604, 2010.
[7] F. Fillion-Gourdeau, H.J. Herrmann, M. Mendoza, S. Palpacelli, and S. Succi, *Formal analogy between the Dirac equation in its Majorana form and the discrete-velocity version of the Boltzmann kinetic equation*, Phys. Rev. Lett., 111, 160602, 2013.
[8] R. Finkelstein, C. Fronsdal, and P. Kaus, *Nonlinear spinor field*, Phys. Rev., 103, 1571–1579, 1956.
[9] R. Finkelstein, R. Lelevier, and M. Ruderman, *Nonlinear spinor fields*, Phys. Rev., 83, 326–332, 1951.
[10] D.J. Gross and A. Neveu, *Dynamical symmetry breaking in asymptotically free field theories*, Phys. Rev. D, 10, 3235–3253, 1974.
[11] F. Gürsey, *On a conform-invariant spinor wave equation*, Nuovo Cimento, 3, 988–1006, 1956.
[12] L.H. Haddad and L.D. Carr, *The nonlinear Dirac equation in Bose-Einstein condensates: Foundation and symmetries*, Physica D, 238, 1413–1421, 2009.
[13] W. Heisenberg, *Quantum theory of fields and elementary particles*, Rev. Mod. Phys., 29, 269–278, 1957.
[14] D.D. Ivanenko, *Notes to the theory of interaction via particles*, Zhurn. Experim. Teoret. Fiz., 8, 260–266, 1938.
[15] S.Y. Lee, T.K. Kuo, and A. Gavrielides, *Exact localized solutions of two-dimensional field theories of massive fermions with Fermi interactions*, Phys. Rev. D, 12, 2249–2253, 1975.
[16] P. Mathieu, *Compact solitons, bags, and radial excitations*, Phys. Rev. D, 32, 3288–3293, 1985.
[17] P. Mathieu, *Soliton solutions for Dirac equations with homogeneous non-linearity in (1+1) dimensions*, J. Phys. A: Math. Gen., 18, L1061–L1066, 1985.
[18] P. Mathieu and T.F. Morris, *Instability of stationary states for nonlinear spinor models with quartic self-interaction*, Phys. Lett. B, 126, 74–76, 1983.
[19] P. Mathieu and R. Saly, *Baglike solutions of a Dirac equation with fractional nonlinearity*, Phys. Rev. D, 29, 2879–2883, 1984.
[20] F.G. Mertens, N.R. Quintero, F. Cooper, A. Khare, and A. Saxena, *Nonlinear Dirac equation solitary waves in external fields*, Phys. Rev. E, 86, 046602, 2012.
[21] Y. Nogami and F.M. Toyama, *Transparent potential for the one-dimensional Dirac equation*, Phys. Rev. A, 45, 5258–5261, 1992.
[22] E.A. Ostrovskaya, Y.S. Kivshar, D.V. Skryabin, and W.J. Firth, *Stability of multihump optical solitons*, Phys. Rev. Lett., 83, 296–299, 1999.
[23] A.F. Rañada, *Relativistic quantum mechanics of the hydrogen atom as the weak-field limit of a nonlinear theory*, Int. J. Theor. Phys., 16, 795–812, 1977.
[24] A.F. Rañada, *Classical nonlinear Dirac field models of extended particles*, in Quantum Theory, Groups, Fields and Particles, A.O. Barut (ed.), Springer, New York, 271–291, 1983.
[25] A.F. Rañada and M.F. Rañada, *Nonlinear model of c-number confined Dirac quarks*, Phys. Rev. D, 29, 985–993, 1984.
[26] B. Saha, *Nonlinear spinor fields and its role in cosmology*, Int. J. Theor. Phys., 51, 1812–1837, 2012.
[27] S.H. Shao, N.R. Quintero, F.G. Mertens, F. Cooper, A. Khare, and A. Saxena, *Stability of solitary waves in the nonlinear Dirac equation with arbitrary nonlinearity*, arXiv:1405.5547v1

[nlin.PS], 2014.
[28] S.H. Shao and H.Z. Tang, *Interaction for the solitary waves of a nonlinear Dirac model*, Phys. Lett. A, 345, 119–128, 2005.
[29] S.H. Shao and H.Z. Tang, *Higher-order accurate Runge-Kutta discontinuous Galerkin methods for a nonlinear Dirac model*, Discrete Cont. Dyn. Syst.-B, 6, 623–640, 2006.
[30] S.H. Shao and H.Z. Tang, *Interaction of solitary waves with a phase shift in a nonlinear Dirac model*, Commun. Comput. Phys., 3, 950–967, 2008.
[31] M. Soler, *Classical, stable, nonlinear spinor field with positive rest energy*, Phys. Rev. D, 1, 2766–2769, 1970.
[32] J. Stubbe, *Exact localized solutions of a family of two-dimensional nonlinear spinor fields*, J. Math. Phys., 27, 2561–2567, 1986.
[33] W.E. Thirring, *A soluble relativistic field theory*, Ann. Phys., 3, 91–112, 1958.
[34] H. Weyl, *A remark on the coupling of gravitation and electron*, Phys. Rev., 77, 699–701, 1950.
[35] J. Xu, S.H. Shao, and H.Z. Tang, *Numerical methods for nonlinear Dirac equation*, J. Comput. Phys., 245, 131–149, 2013.